Received February 8, 2021, accepted February 19, 2021, date of publication February 23, 2021, date of current version March 3, 2021.

Digital Object Identifier 10.1109/ACCESS.2021.3061340

An MPPT Algorithm for PV Systems Based on a Simplified Photo-Diode Model

CARLOS RESTREPO[1], CATALINA GONZÁLEZ-CASTAÑO[2], JAVIER MUÑOZ[1], (Member, IEEE), ANDRII CHUB[3], (Senior Member, IEEE), ENRIC VIDAL-IDIARTE[4], (Member, IEEE), AND ROBERTO GIRAL[4], (Senior Member, IEEE)

[1]Department of Electromechanics and Energy Conversion, Universidad de Talca, Curicó 3340000, Chile
[2]Department of Engineering Sciences, Universidad Andres Bello, Santiago 7500971, Chile
[3]Department of Electrical Power Engineering and Mechatronics, Tallinn University of Technology, 19086 Tallinn, Estonia
[4]Departament d'Enginyeria Electrònica, Elèctrica i Automàtica, Escola Tècnica Superior d'Enginyeria, Universitat Rovira i Virgili, 43003 Tarragona, Spain

Corresponding author: Roberto Giral (roberto.giral@urv.cat)

This work was supported in part by the Chilean Government under Project CONICYT/FONDECYT 1191680, in part by the SERC Chile Project under Grant CONICYT/FONDAP/15110019, in part by the Spanish Agencia Estatal de Investigación and the Fondo Europeo de Desarrollo Regional (AEI/FEDER, UE) under Project DPI2016-80491-Rand DPI2017-84572-C2-1-R, in part by the Estonian Research Council under Grant PSG206, and in part by the Estonian Centre of Excellence in Zero Energy and Resource Efficient Smart Buildings and Districts, European Regional Development Fund, under Grant 2014-2020.4.01.15-0016.

ABSTRACT A Maximum Power Point Tracking (MPPT) algorithm is proposed based on the assumption that a simplified three-parameter photodiode-based model can provide an excellent approximation of a PV module $i-v$ curve around its maximum power point (MPP). Procedures to obtain the MPP coordinates and the three parameters of the approximated $i-v$ curve from experimental online measurements, analytical and Newton-Raphson iterative calculations are thoroughly described. Initializing the model as well as optimizing it to operate faster by identifying only subsets of the model parameters provides excellent MPPT efficiency in both static and dynamical MPPT situations. The performance of the proposed algorithm has been verified in comparison with other well-known MPPT methods using the software-in-the-loop approach. Next, its performance has been evaluated by using the MATLAB-based hardware-in-the loop experimental setup that provides the required reproducibility of the different synthetic and real irradiance and temperature profiles considered.

INDEX TERMS Photovoltaic energy, maximum power point tracking, photodiode model.

NOTATION

Term	Description
MPP	Maximum power point.
MPPT	Maximum power point tracking.
η_{PV}	Global efficiency of the PV system.
η_{Conv}	Power conversion efficiency.
η_{MPPT}	Maximum power conversion tracking efficiency.
i_{MPP}	Current at the MPP of the PV module.
v_{MPP}	Voltage at the MPP of the PV module.
I_{SC}	Short-circuit photogenerated current.
I_R	Reverse saturation current.
a	Temperature dependent voltage factor.
$lnIR$	Natural logarithm of I_R.
i_{MPPt}	Theoretical value of i_{MPP}.
v_{MPPt}	Theoretical value of v_{MPP}.
ΔV	Distance between voltage points.
ΔI	Current threshold.
(v_1, i_1)	Three points of the $i-v$ curve used
(v_2, i_2)	in the three-points procedure.
(v_3, i_3)	
(v_a, i_a)	Two points of the $i-v$ curve used
(v_b, i_b)	in the two-points procedure.
NR	Newton-Raphson

The associate editor coordinating the review of this manuscript and approving it for publication was Ahmed F. Zobaa.

I. INTRODUCTION

The technology of solar photovoltaic (PV) modules showed impressive developments in the past decades. As a result, the cost of PV modules had reduced remarkably down to 30 ¢/W, which is a thirty-fold drop from the prices of a decade ago [1]. This resulted from the increased efficiency of the PV cells, scaling up of their production, as well as an increase

in the nameplate power of PV modules [2]. Consequently, the installed power grew fourteen-fold and the global average levelized cost of electricity dropped roughly five-fold down to 7 ¢/kWh in the last decade. Considering these advancements and predicted further reduction of the capital and operating costs along with the abundance of sunlight, the solar energy is considered a promising solution that could take over the electricity generation industry [3].

The output power of a PV system depends on operating conditions and system components that perform energy conversion. The efficiency of PV modules depends on PV cell technology utilized inside and generally correspond to over 20% for monocrystalline-Si-based PV modules that dominate on the PV market [2]. In outdoor conditions, this efficiency decreases gradually due to the degradation of PV cells with annual rate reported in the range between 0.22 %/year [4] and 1 %/year [5]. Therefore, the overall performance of an installed PV system is defined by its architecture and power electronic converters employed. Hence, significant research efforts were focused on power electronic converters for PV applications. To maximize electric energy conversion efficiency, in PV systems the transformerless inverters with the efficiency of up to 99 % are used in grid-connected applications [6], while DC-DC converters could be used additionally for maximum power point tracking (MPPT) at PV module- or string-level [7], [8]. Moreover, these converters have to provide a long lifetime despite operating in harsh climatic conditions at elevated temperatures [9], [10].

At the same time, standards like EN 50530 define overall efficiency of PV converters η_{PV} as the product of the converter efficiency η_{Conv}, i.e., the ratio between the output and the input power, and the MPPT efficiency η_{MPPT}, i.e., the ratio between the power drawn by a converter from a PV module and the maximum PV power available from this module [11]:

$$\eta_{PV} = \eta_{Conv} \cdot \eta_{MPPT}. \tag{1}$$

Therefore, the MPPT efficiency has to be high in both static and especially dynamic operating conditions to ensure high overall performance of a PV system. It was demonstrated in [12] that a highly-efficient converter can demonstrate poor overall performance if its MPPT efficiency is low.

There are numerous MPPT methods available, which could be broadly categorized as on- and off-line methods. The online methods, like hill-climbing algorithm, are typically perform a search of the maximum power point (MPP) based on the measured instantaneous values of current, voltage, temperature, solar irradiance, and other physical parameters as well as their preceding measured values [13]. The abundant availability of different MPPT methods makes it difficult to select one suitable for a particular application and thus holds back their wider industrial adoption [14]. Many of them depend in the PV array configuration and may require knowledge of some of its parameters to achieve high MPPT efficiency, which the applicability of such MPPT methods [15]. Therefore, the conventional iterative search methods and their improved versions stay popular in research and practice as they provide an acceptable cost of realization and high MPPT efficiency [16]. On the other hand, the conventional iterative MPPT methods, like perturb and observe (P&O), could show poor MPPT performance under fast-changing operating conditions [17], [18]. There is a group of MPPT methods based on an analytical description of the PV cell physical model, such as β-parameter based MPPT method [19]. They can provide good convergence and high MPPT efficiency but may require higher computational resources than simpler counterparts [16], [20].

This article is focused on analytical MPPT methods that are based on modeling or approximation of PV module $i - v$ characteristics. Typically they are based on a single- or dual-photodiode model of a PV cell. Universal implementation of such MPPT algorithms requires on-line identification of parameters of a PV cell model [21]. Identification of the MPP current and voltage values could require use of special techniques like Lambert W_0 function [21] or soft-computing algorithms [22]. Both approaches could be time-consuming, even more so for these special functions that are calculated using computational methods, like Halley's or Fritsch's iterations [23]. To improve convergence speed after irradiance disturbances, the computational burden of these analytical methods has to be reduced. Sixth order polynomial approximation of the photodiode model was used with the Newton–Raphson (bisection) numerical method in [24] based on measurements of three operating points, which allowed for a reduction of the MPPT computational requirements. On the other hand, a polynomial approximation loses the physical meaning of the processes in PV cells.

This work demonstrated that measurements in three operating points proposed in [24] are needed only at the start-up, once a day or when shading conditions are detected. This assumption is based on the fact that some parameters of the photodiode model are virtually constant within a day due to the very slow degradation of PV modules [4], [5]. Hence, using measurements in two operating points is usually sufficient for the estimation of the photodiode model parameters. It allows for fast convergence of the simple Newton–Raphson method despite considering the classical non-linear mathematical model of a photodiode instead of its approximations. The proposed two-point algorithm has to be run again only after a change in the operating conditions is detected from measurements of the converter input current and voltage. Therefore, the resulting two-point algorithm will be very fast and would improve the MPPT efficiency, especially under fast-changing operating conditions.A preliminary modified version of the procedure to operate in shading conditions, based on the measurements in three operating points, is also proposed assuming that under shading conditions large current variations will be detected.

The main goal of this work is to verify if the proposed MPPT method based in the experimental on-line identification of the simplified single diode model of the PV module is very competitive in terms of MPPT efficiency in comparison

with other highly efficient reported methods. The main contributions of this article are the following:

- A comprehensive theoretical review of the main algorithms required to identify the single-diode model parameter of the PV module allows to configure a fast identification procedure that requires only two experimental points of the $i - v$ curve. Frequently, the coordinates of the second point are coincident or very close to those of a new MPP point, which also contributes to increase the MPPT efficiency.
- In static and slow varying irradiance and temperature conditions, the MPPT efficiency is better than the provided by methods because there is not a continuous variation of the operation point around the MPP. While the experimental MPP current coordinate is in good agreement with the theoretical prediction provided by the model, the voltage coordinate is kept at a constant value and only the current is monitored until the error between predicted and experimental MPP current values reaches a threshold.
- In fast varying conditions, the requirement of only two valid points of the $i - v$ curve to identify the model parameters accurately enough is more probable thus resulting in a fast and more robust identification of the experimental MPP, which provides better efficiency than other methods.
- The MPPT performance of the method has been verified through hardware-in-the loop experiments and simulations that offer good accuracy and reproducibility.
- Preliminary tests have shown that the method can be adapted to shading conditions.

The remaining of this article is organized as follows: The second section formulates the MPPT target in terms of the conventional one-diode model of a PV cell. The third section describes the proposed MPPT. Next, the comparative simulation results are provided for the proposed and several existing MPPT methods in the fourth section. The fifth section provides experimental results demonstrating the performance of the proposed MPPT method for the two daily mission profiles. In the sixth section simulations results corresponding to preliminary modifications of the algorithms to take into account shading conditions are presented. After that, the conclusions are drawn.

II. DIODE BASED MODEL MPPT DESCRIPTION

The MPPT method is based on modeling the PV module $i-v$ characteristics in the vicinity of the maximum power point by the single photo-diode basic model given as:

$$i_{pv} = I_{SC} - I_R e^{a \cdot v_{pv}}, \tag{2}$$

where I_{SC}, I_R and a are parameters dependent on the module technology (type of cells, area of cells, number of cells in series, etc.), as well as on the irradiance and operating temperature. For more details about PV mathematical models with a high accuracy that can be easily solved by analytical methods for real-time identification, see [24]–[27].

The electric power $P_{pv} = i_{pv} \cdot v_{pv}$ delivered by the solar module can be expressed in terms of the module current as

$$P_{pv} = i_{pv} \frac{ln(I_{SC} - i_{pv}) - lnIR}{a}, \tag{3}$$

where the parameter $lnIR$ is used instead of the natural logarithm of the reverse saturation current $lnIR = ln(I_R)$.

$$\frac{dP_{pv}}{di_{pv}} = \frac{1}{a}\left(ln(I_{SC} - i_{pv}) - lnIR - \frac{i_{pv}}{I_{SC} - i_{pv}}\right) \tag{4}$$

Therefore, the current coordinate of the maximum power point (i_{MPP}) can be obtained by numerically solving (5), which only depends on parameters I_{SC} and $lnIR$.

$$f(i_{MPP}) = ln(I_{SC} - i_{MPP}) - lnIR - \frac{i_{MPP}}{I_{SC} - i_{MPP}} = 0 \tag{5}$$

A simple Newton-Raphson (NR) algorithm yields i_{MPP} after a few iterations, provided that the seed value (6) is selected. The seed value is obtained by neglecting the term $ln(I_{SC} - i_{MPP})$ in (5):

$$i_{MPP}[0] = \frac{-lnIR}{1 - lnIR} I_{SC}, \tag{6}$$

$$i_{MPP}[n+1] = i_{MPP}[n] - \frac{f(i_{MPP}[n])}{\dot{f}(I_{SC}[n])}, \tag{7}$$

where the derivative of $f(i_{MPP})$ is

$$\dot{f}(i_{MPP}) = \frac{df(i_{MPP}}{di_{MPP}} = \frac{i_{MPP} - 2I_{SC}}{(I_{SC} - i_{MPP})^2}. \tag{8}$$

Finally, the voltage coordinate of the maximum power point (v_{MPP}), which will be used as the voltage reference of the dc-dc converter that regulates the PV module voltage, can be obtained as

$$v_{MPP} = \frac{ln(I_{SC} - i_{MPP}) - lnIR}{a}. \tag{9}$$

The core of the MPPT algorithm consists in determining the three parameters of the diode model as they vary depending on the irradiance and cell temperature of the PV module. An initial approach requires knowing the current and voltage coordinates of three operating points in the vicinity of the MPP so that the model is well fitted around it. The coordinates of the three points have to be different enough so that the three parameters can be determined correctly. The procedure to obtain the three parameters ($lnIR$, a, and I_{SC}) has been named Three-Points.

As it will become apparent later, the parameter $lnIR$ is mainly related to the PV cell technology (fill factor) and aging, and its dependence on the temperature and irradiance can be neglected. In a similar manner, it can be considered that the variations of the parameter I_{SC} are caused mainly by irradiance changes, while the parameter a reflects the temperature-related effects. In most cases, these considerations allow obtaining parameter $lnIR$ in a daily (or even weekly or monthly) basis. Therefore, the Three-Points algorithm will be used mainly to initialize the model at dawn. It can be also useful to reinitialize the model parameters if a watch-dog safeguard is implemented.

If the parameter *lnIR* is considered constant, the coordinates of only two points near the MPP will be sufficient to model a static $i - v$ curve. The procedure of obtaining the parameters a and I_{SC} in this way has been named Two-Points. In very variable operating conditions, when the irradiance can vary much faster than the temperature, the estimation of the MPP coordinates through determining just I_{SC} can be a sensible/useful approach. As will be shown, this consideration has been taken into account inside the Two-Points algorithm.

III. MPPT PROPOSED ALGORITHM

In the following subsections, we will describe the main aspects of the algorithm. Namely, the mathematical aspects of determining the model parameters and the calculations required to determine the MPP of a static $i-v$ curve. Since the $i - v$ curves are dependent on the irradiance and temperature levels, there are also important aspects of the procedures to deal with the problems that arise when the points measured correspond to different $i - v$ curves. As an example, some calculations require the computations of expressions of the form $ln(I_{SC} - i_{MPP})$, where the measurements performed to determine I_{SC} could correspond to one $i - v$ curve and i_{MPP} could correspond to another, sometimes very different, curve because of a fast irradiance change between measurements (clouds covering the PV module on a windy day). If the irradiance has increased when measuring i_{MPP}, it is quite possible that $I_{SC} - i_{MPP} < 0$, which could cause havoc in the logarithm computation. In similar atmospheric conditions, the probability of obtaining wrong results will be more significant in the procedure involving the measurements of three different (v, i) points than in the case of just requiring two points. This is why the Two-Points procedure is preferred over the Three-Points one after the start-up initialization.

A. THREE-POINTS PROCEDURE

As it has been mentioned previously, the Three-Points procedure will be used mainly to initialize the diode-model parameters and, in particular, parameter *lnIR*. To provide useful parameters, the procedure requires several conditions: a) that the coordinates of three points are from the same static $i - v$ curve, b) that the three different operating points are in the vicinity of the MPP, and c) that the current coordinates of the three points are above a predetermined minimum level (dawn) and different enough so that their differences are also above a predetermined level. To make sure that condition a) holds true for MPPT in severely dynamic operating conditions, the parameter *lnIR* can be initialized from the manufacturer data-sheet or stored from previous days. In some cases, in which the position of the MPP point (irradiance and temperature) vary slowly, the three initial parameters of the diode model can be found by averaging the results obtained from several consecutive runs of the Three-Points algorithm in which, in addition, inconsistent sets of the three points are discarded. Condition b) can be ensured either by using three points that are separated by considerable voltage steps or by using another MPPT algorithm such as the classical Perturb and Observe (P&O). The latter approach was preferred and implemented in this article. Finally, condition c) requires condition b) to be true and selecting appropriate limits to decide if the three currents are sufficiently large and different from each other. Satisfying this conditions would be closely related with the resolution of the input current sensor.

Algorithm 1: Three-Points Procedure

Result: I_{SC}, a, $lnIR$, i_{MPPt}, v_{MPPt}
$v_M = v_{MPPt}$;
Error = true;
while *Error* **do**
  Error = false;
  $v1 = vM \times 1.03$; $v3 = vM \times 0.97$; $v2 = vM$;
  Write-V(v_1); i_1 = Read-IV;
  Write-V(v_3); i_3 = Read-IV;
  Write-V(v_2); i_2 = Read-IV;
  if *($i_1 > i_2$) or ($i_2 > i_3$) or (any current is outside expected range)* **then**
    Error = true;
  else
    (24) $I_{SC} = \frac{i_2^2 - i_1\, i_3}{2\, i_2 - (i_1 + i_3)}$;
    if *($I_{SC} < i_1$) or ($I_{SC} < i_2$) or ($I_{SC} < i_3$)* **then**
      Error = true;
    else
      (19) $a = \frac{ln(I_{SC} - i_1) - ln(I_{SC} - i_2)}{v_1 - v_2}$;
      (20) $lnIR = \frac{v_2 \cdot ln(I_{SC} - i_1) - v_1 \cdot ln(I_{SC} - i_2)}{v_2 - v_1}$;
      if *(a is outside expected range)* **then**
        Error = true;
      end
      if *(lnIR is outside expected range)* **then**
        Error = true;
      end
    end
  end
end
(7) $i_{MPPt} = $ Newton-Raphson($lnIR$, I_{SC});
(9) $v_{MPPt} = (ln(I_{SC} - i_{MPP}) - lnIR)\,/a$;

Let us assume that the three points (v_1, i_1), (v_2, i_2), (v_3, i_3) are near the MPP and that are monotonically distributed (consistent) so that $v_1 > v_2 > v_3$ and $i_1 < i_2 < i_3$. We can build the following set of equations in logarithmic form:

$$ln(I_{SC} - i_1) = lnIR + a \cdot v_1, \tag{10}$$
$$ln(I_{SC} - i_2) = lnIR + a \cdot v_2, \tag{11}$$
$$ln(I_{SC} - i_3) = lnIR + a \cdot v_3. \tag{12}$$

Subtracting equation (11) from (10), and (12) from (11), we eliminate the parameter *lnIR*:

$$ln(I_{SC} - i_1) - ln(I_{SC} - i_2) = a \cdot (v_1 - v_2), \tag{13}$$
$$ln(I_{SC} - i_2) - ln(I_{SC} - i_3) = a \cdot (v_2 - v_3). \tag{14}$$

Dividing the equations (13) and (14) to eliminate the coefficient a results in the following equation:

$$\frac{ln(I_{SC}-i_1)-ln(I_{SC}-i_2)}{ln(I_{SC}-i_2)-ln(I_{SC}-i_3)}=\frac{v_1-v_2}{v_2-v_3}. \tag{15}$$

In the cases when equation (15) has no analytical solutions, the parameter I_{SC} can be determined, for instance, using another Newton-Raphson (NR) numerical procedure. For this purpose, the equation can be rewritten as

$$\begin{aligned} f(I_{SC}) = {} & (v_1-v_2)\cdot ln(I_{SC}-i_3) \\ & +(v_3-v_1)\cdot ln(I_{SC}-i_2) \\ & +(v_2-v_3)\cdot ln(I_{SC}-i_1)=0, \end{aligned} \tag{16}$$

the derivative of which can be calculated as follows:

$$\dot{f}(I_{SC})=\frac{df(I_{SC})}{dI_{SC}}=\frac{v_1-v_2}{I_{SC}-i_3}+\frac{v_3-v_1}{I_{SC}-i_2}+\frac{v_2-v_3}{I_{SC}-i_1}. \tag{17}$$

The short circuit current could be found by iterating the expression

$$I_{SC}[n+1]=I_{SC}[n]-\frac{f(I_{SC}[n])}{\dot{f}(I_{SC}[n])} \tag{18}$$

with an initial seed value of $I_{SC}[0]=i_3+\epsilon$. Once I_{SC} has been obtained, the parameter a can be easily determined from (13) (or from (14)) as

$$a=\frac{ln(I_{SC}-i_1)-ln(I_{SC}-i_2)}{v_1-v_2}, \tag{19}$$

while $lnIR=ln(I_{SC}-i_x)-a\cdot v_x$; $(x=1,2 \text{ or } 3)$ or it can also be obtained, for instance, as

$$lnIR=\frac{v_2\cdot ln(I_{SC}-i_1)-v_1\cdot ln(I_{SC}-i_2)}{v_2-v_1}. \tag{20}$$

It is worth noting that the purpose of the procedure is to model the $i-v$ curve around the MPP so that the parameters obtained when using the usual three points provided by the manufacturers, namely $(0, I_{SC})$, (v_{MPP}, i_{MPP}), $(V_{OC}, 0)$, can provide I_{SC} values very different from the nominal ones used in the calculations, which depends on the PV module fill factor.

An interesting possibility is to use a middle point equidistant in voltage from the other two ($v_2=(v_1+v_3)/2$). In this case, $v_2=v_3+\Delta V$, $v_1=v_2+\Delta V$, and equation (16) can be solved analytically as it is shown next. ΔV can be a percentage of the nominal v_{MPP}, for instance, 2 %, or a fixed value.

$$\begin{aligned} f(I_{SC}) = {} & \Delta V\cdot(ln(I_{SC}-i_3)-2\cdot ln(I_{SC}-i_2) \\ & +ln(I_{SC}-i_1))=0 \end{aligned} \tag{21}$$

$$f_2(I_{SC})=ln\left(\frac{(I_{SC}-i_3)(I_{SC}-i_1)}{(I_{SC}-i_2)^2}\right)=0 \tag{22}$$

$$\frac{(I_{SC}-i_3)(I_{SC}-i_1)}{(I_{SC}-i_2)^2}=1 \tag{23}$$

$$I_{SC}=\frac{i_2^2-i_1i_3}{2i_2-(i_1+i_3)} \tag{24}$$

Once I_{SC} has been determined using (24), the remaining parameters of the photodiode model can be obtained from the equations (19) and (20), as can be seen in Algorithm 1. Finally, the NR algorithm in (5)-(8) and expression (9) will be used to get the MPP coordinates.

B. TWO-POINTS PROCEDURE

As was mentioned previously, if the parameter *lnIR* is considered constant, obtaining the remaining parameters of the simplified photodiode $i-v$ static model requires only two points. Problems arise, however, if the $i-v$ curve changes between measurements, and each point corresponds to a different static $i-v$ curve. In this case, one point has to be discarded, and additional measurements are needed. Also, if the measured current in the selected point is too small, a new point has to be found by selecting a different voltage coordinate to measure a suitable current value. In addition, to provide the new values of parameters I_{SC} and a, other outputs of the Two-Points Procedure are the theoretical coordinates of the MPP (v_{MPPt}, i_{MPPt}), as in the case of the Three-Points Procedure. Although there are some conditions that are evaluated inside the Two-Points procedure, the main validation of the $i-v$ curve model is performed in the Main Procedure, where the measured current (i_{MPP}) at the theoretical MPP defined by voltage coordinate v_{MPPt} is continuously compared with the theoretical value (i_{MPPt}) calculated in the Two-Points procedure. When the modulus of the difference between the measured and the theoretical values of the current reaches the threshold $(|i_{MPP}-i_{MPPt}|>\Delta I)$, the Two-Points Procedure is executed again. The threshold can be reached as a consequence of irradiance/temperature changes if the previous $i-v$ curve parameters have been correctly obtained or if the MPP predicted in the previous Two-Points iteration is incorrect as a result of the irradiance/temperatures variations during the parameter identification.

The first point (v_a, i_a) in the procedure is the last measured point at the MPP voltage coordinate $(v_a=v_{MPPt}, i_a=i_{MPP})$. Therefore, only one measurement is needed to obtain the second point (v_b, i_b). Next, there are two possibilities of obtaining these coordinates:

(a) assuming that only irradiance has changed, the short circuit current can be calculated as $(I_{SC}=i_a+e^{lnIR+a\cdot v_a})$, which allows for computing the current coordinate using the NR iterative process already described and getting the voltage coordinate using (9);
(b) to calculate its voltage coordinate as $v_b=v_a\pm\Delta V$, adding the positive ΔV if $(i_a>i_{MPPt})$ or subtracting it in the opposite case. ΔV can be a fraction of the previous MPP voltage, for instance, a 2 %, or the same used in the Three-Points procedure.

A possible issue in using the option a) is that, in many cases, v_b is very close to v_a and the two currents are too similar. Although the option b) can be selected directly, we believe that the option a) is interesting for irradiance mission profiles with large changes. Hence, the option a) was implemented

here for calculation of the second point when the values i_b and i_a are too close. Apart from evaluating that value i_b is not too small, the option a) requires the two voltage coordinates to be close to each other by limiting v_b so that, for instance, $|v_b - v_a| < v_a/10$. Another sensible precaution is to check if the points correspond to a monotonically decreasing $i - v$ curve.

Since the voltage coordinate of the point b could be higher or smaller than that of the point a, they may need to be reordered as $v_a < v_b$, after what the condition $i_a > i_b$ is tested. The mathematical expressions involved in the typical routine are described below.

The photo-diode equations for two operating points are

$$i_a = I_{SC} - e^{lnIR + a \cdot v_a}, \tag{25}$$
$$i_b = I_{SC} - e^{lnIR + a \cdot v_b}. \tag{26}$$

In the identification of parameters, there are two possibilities. The first one is obtaining the parameter a first and use it to calculate I_{SC}, while in the second possibility is to obtain the parameter I_{SC} before a. The preferred option is to obtain the parameter a first. By subtracting the previous equations, we obtained an implicit function of parameter a that can be solved by the NR method. The function and its derivative are described by (27) and (28), respectively.

$$f(a) = (i_a - i_b) + e^{lnIR + a \cdot v_a} - e^{lnIR + a \cdot v_b} = 0 \tag{27}$$
$$\dot{f}(a) = \frac{df(a)}{da} = v_a e^{lnIR + a \cdot v_a} - v_b e^{lnIR + a \cdot v_b} \tag{28}$$

The seed value for the NR iteration is the previous value of a, ($a[0] = a$).

$$a[n+1] = a[n] - \frac{f(a[n])}{\dot{f}(a[n])} \tag{29}$$

As it is shown in Algorithm 2, once a has been obtained with the desired resolution, I_{SC} is obtained from (25), or (26), or their combination as in

In the case when it is decided to calculate I_{SC} before a, the diode equations (25) and (26) are rewritten to explicit a as

$$a = \frac{ln(I_{SC} - i_a) - lnIR}{v_a} = \frac{ln(I_{SC} - i_b) - lnIR}{v_b}. \tag{30}$$

Similarly to the previous case, parameter I_{SC} can be obtained by NR iterations of the function obtained from (30):

$$f_3(I_{SC}) = v_a \cdot (ln(I_{SC} - i_b) - lnIR) - v_b \cdot (ln(I_{SC} - i_a) - lnIR) = 0, \tag{31}$$
$$\dot{f}_3(I_{SC}) = \frac{df_3(I_{SC})}{dI_{SC}} = \frac{v_b}{I_{SC} - i_a} - \frac{v_a}{I_{SC} - i_b}, \tag{32}$$
$$I_{SC}[1] = i_a + \epsilon, \tag{33}$$
$$I_{SC}[n+1] = I_{SC}[n] - \frac{f_3(I_{SC}[n])}{\dot{f}_3(I_{SC}[n])}. \tag{34}$$

Finally, in this second case, a can be obtained easily from (30).

$$I_{SC} = \frac{i_a + e^{lnIR + a \cdot v_a} + i_b + e^{lnIR + a \cdot v_b}}{2}. \tag{35}$$

Algorithm 2: Two-Points Procedure

Result: I_{SC}, a
$v_a = v_{MPPt}$;
Error = true;
while *Error* **do**
  Error = false;
  i_a = Read-IV;
  while $i_a < \Delta I$ **do**
    $v_a = 0.75 \times v_a$;
    Write-V(v_a); i_a = Read-IV;
  end
  $I_{SC} = i_a + e^{lnIR + a \cdot v_a}$;
  (7) i_b = Newton-Raphson($lnIR$, I_{SC});
  (9) $v_b = (ln(I_{SC} - i_b) - lnIR)/a$;
  if *($v_b > v_a$ and v_b is outside expected range)* **then**
    $v_b = min(v_a + N \times \Delta V,\ v_{Max})$; $(N = 8)$;
  else
    if *($v_b < v_a$ and v_b is outside expected range)* **then**
      $v_b = max(v_a - N \times \Delta V,\ v_{Min})$; $(N = 8)$;
    end
  end
  Write-V(v_b); i_b = Read-IV;
  while $i_b \approx i_a$ **do**
    $v_b = v_b + sign(v_b - v_a) \times \Delta V$;
    Write-V(v_b); i_b = Read-IV;
  end
  if *($v_b < v_a$)* **then**
    SwapPoints so that ($v_a < v_b$);
  end
  if *($i_a < i_b$)* **then**
    Error = true;
  else
    (29) a = Newton-Raphson(v_a, i_a, v_b, i_b);
    $I_{SC} = i_a + e^{lnIR + a \cdot v_a}$;
  end
end

C. MAIN PROCEDURE

The main algorithm has an initial part in which there is an initialization of variables and constants, and communications if required. The initialization part continues with the execution of an auxiliary procedure (Wait-for-Dawn) that, at the moment, assumes that the system is started at dawn and waits for the current levels around the MPP to reach a sufficiently large value so that the Three-Points procedure will provide a reasonable estimation of the parameter $lnIR$. Among many possibilities of designing the Wait-for-Dawn procedure, it was decided to use a classical Perturb-and-Observe (P&O) MPPT procedure until the current around the MPP goes above 360 mA, which is about 7 times the current threshold $\Delta I = 50$ mA used in the program decisions and comparisons involving current levels. Moreover, this

current level roughly corresponds to the solar irradiance of roughly 150 W/m^2, which is below typical daytime diffused irradiance on cloudy days and thus ensures the use of the initialization algorithm only at dawn. The measured current is considered too low if it is under ΔI. Similarly, two currents are considered equal if the modulus of their difference is less than ΔI.

The voltage increment ΔV of the basic P&O used in the Wait-for-Dawn procedure as well as in the Two-Point and Three-Points Procedures has been adjusted by taking into account the characteristics of the PV module type that has been considered in the dynamic MPPT tests, a HIT ® N330 PV module from Panasonic. Initially we considered a value of 1.16 V for ΔV, a 2% of the MPPT voltage of the PV module at Standard Test Conditions (STC), which is 58 V. Later, it was decided to carry out a set of simulations using the Three-Points Procedure to locate the MPP of the module at different temperature and irradiance operating points. The starting voltage coordinate of the simulations was the average of all MPP voltages, 57.46 V. The performance of the algorithm was tested for values of ΔV ranging from almost zero to 5 V. The results obtained are summarized in Figure 1. The bottom and left axis show the different values of irradiance and temperature. At the coordinates of each operation point there is a circle whose color corresponds with the value of ΔV yielding the minimum absolute error between the simulated MPP and the provided by the Three-Points Procedure. The right axis shows a color bar with the tested ΔV values. The diameter of the larger circles is proportional to the error. A minimum diameter has been given to too small circles so that their color can be seen. The maximum error was 410 mV and the minimum error about 100 μV. Since the average value of all optimum ΔV values in the figure is about 995 mV, a rounded value of $\Delta V = 1$ V has been selected for all algorithms.

The procedure to determine ΔI is quite different from the followed to choose ΔV. In this case different simulations of the Two-Point MPPT procedure were carried out at different irradiation and temperatures whose results are plotted in Figure 2. Boxplots corresponding to four different temperatures have been obtained considering discrete ΔI values ranging from 25 mA to 150 mA and separated by 25 mA. The vertical axis shows around the MPP point the value of the corresponding irradiance variation that triggers a new Two-Point MPP search. We have selected a value of $\Delta I = 50$ mA that triggers the MPP algorithm for average values of irradiance changes of about 8.7 W/m^2, less than 1% of 1 kW/m^2. Larger values of ΔI would imply larger irradiance thresholds, which could affect negatively MPPT efficiencies in fast-varying temperature but slow-varying irradiation conditions in which the voltage coordinate of the MPP experiments fast variations but the current coordinate doesn't. Smaller ΔIs would trigger the algorithm more frequently, which could also affect the efficiency because of the Two-Points algorithm sometimes imposes an operating point slightly away from the MPP, which could be unnecessary in slow-varying irradiation and temperature conditions in which the voltage coordinate of the MPP varies also slowly. This parameter must probably be tuned according to the prevalent atmospheric conditions of the site in which the module is placed.

As it was decided, the parameter *lnIR* is estimated only at the initialization section. In addition, it is very important to obtain a good estimation. Therefore, the Three-Points procedure is executed sequentially four times. The four results are averaged to obtain the initial set of parameters of the photodiode equation that approximates i-v characteristics of the PV module. Alternative and/or additional solutions can be also implemented, such as obtaining the initial parameters offline from the manufacturer data, executing the procedure until the parameters of two consecutive procedures are almost equal, using some of the parameters stored from previous days, or a combination of several of these solutions. Hence, the initialization section finishes by providing the theoretical coordinates of the MPP (v_{MPPt}, i_{MPPt}) and setting the voltage reference with v_{MPP}.

Once the initialization has been completed, there is a loop that lasts until the "end of the day" in which the current (i_{MPP}) corresponding to the theoretical MPP voltage is measured continuously until it differs significantly from the theoretical value (i_{MPPt}) provided by the Two-Point procedure. When the magnitude of the difference between the two currents reaches the ΔI threshold new coordinates for the theoretical MPP are calculated, which requires using the Two-Point procedure to estimate again a and I_{SC}, and from them i_{MPPt} and v_{MPPt}. The pseudo-code algorithm of the Main procedure is listed as Algorithm 3.

Algorithm 3: Main Procedure

```
Result: Operates the PV module at its MPP
Initialization (variables, constants, communications);
Wait-for-Dawn (P&O);
Three-Points Procedure;
while Not(End-of-Day) do
    while (i_MPP ≈ i_MPPt) do
        i_MPP = Read-IV;
    end
    if (abs(i_MPP − i_MPPt) > Shading − threshold then
        Shading-conditions Procedure;
    end
    Two-Points Procedure;
    (7) i_MPPt = Newton-Raphson(lnIR, I_SC);
    (9) v_MPPt = (ln(I_SC − i_MPP) − lnIR) /a;
    Write-V(v_MPPt);
end
```

IV. SOFTWARE-IN-THE-LOOP (SIL) TESTING

A comparative study of the proposed MPPT method with other relevant algorithms proposed in the literature is presented in this section. Each of the proposed MPPT algorithms

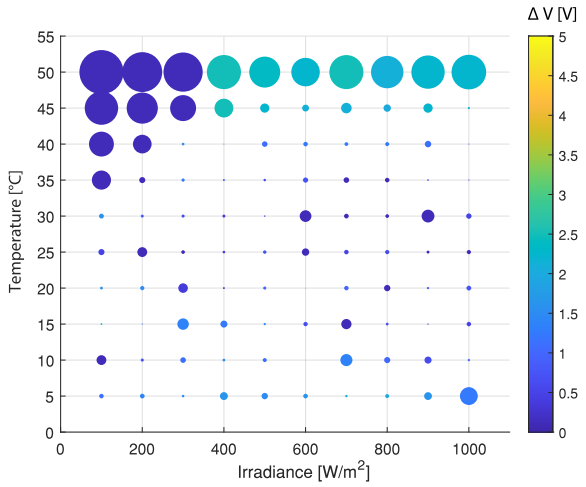

FIGURE 1. Map of minimum absolute errors between exact MPP voltage coordinates and the provided by the Three-Point MPPT procedure in a N300 PV module. The color of the circles indicates the optimum ΔV values used at the Three-Point procedure while their diameter is proportional to the error.

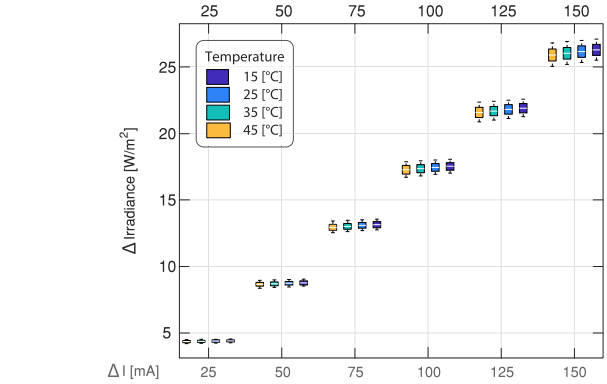

Δ I [mA]	25	50	75	100	125	150
Upper adjacent [W/m^2]	4.5187	9.0298	13.5432	18.0588	22.5767	27.097
75th percentile [W/m^2]	4.4227	8.8475	13.2710	17.6947	22.1185	26.5426
Median [W/m^2]	4.3472	8.6954	13.0436	17.3915	21.7391	26.0866
25th percentile [W/m^2]	4.2749	8.5503	12.8255	17.1007	21.3759	25.6509
Lower adjacent [W/m^2]	4.1761	8.3528	12.5292	16.7053	20.8812	25.0567

FIGURE 2. Boxplots representing the threshold irradiation changes that trigger the Two-Point MPPT algorithm as a function of ΔI and considering the ambient temperature as a parameter. Four different values of the ambient temperature have been considered in the simulations.

was implemented in PSIM by means of a simplified C block that allows for using a custom C code directly without compiling it. This advantage allows for incorporating external C code, as used in a digital signal controller (DSC), into a simulation model whereby comparisons between the different MPPT techniques can be easily made. In addition, most of the major simulation software supports C code, such as PLECS, PSIM, MATLAB etc. Therefore, the digital MPPT algorithms presented in this section can be extended to other simulation programs in a simple way. In the following subsections, a description of the MPPT methods used to carry out the comparison with the proposed algorithm is presented. The MPPT methods include extremum seeking control (ESC) techniques (FESC, SM-ESC, SMPPT), and perturb and observe (P&O) algorithm, and their description will be given below. The selected algorithms present different speeds of convergence and thus allow for proper benchmarking versus the proposed one. It is worth mentioning that all simulations in this section take into account discrete nature of modern MPPT implementations with a DSC by introducing zero-order hold with 1 kHz sampling frequency for measured voltage and current of the PV module.

A. LOSS-FREE RESISTOR BASED ON ESC (FESC) METHOD

The FESC method was introduced for photovoltaic application in [28]. This is an ESC technique, and its objective is to obtain a conductance value from the power time of the PV. The power P_{pv} can be expressed as a function of the LFR (loss-free resistor) conductance g as

$$P_{pv} = g v_{pv}^2. \tag{36}$$

The MPPT algorithm uses a hysteresis comparator that generates a binary signal showing the sign of the power derivative. This binary signal is the input to a logic circuit with a delay τ_d. The minimum time delay τ_d can be defined as

$$\tau_d \geq 5 r_{max} C_p, \tag{37}$$

where r_{max} $(1/g_{max})$ is the maximum resistor value from the MPPT algorithm, taking into account the point where the PV characteristic presents the MPP at the highest current and the lowest voltage. The settling time of the PV voltage and current are directly related to the capacitor C_p of the PV module/string. After a fixed time interval, the logic circuit establishes if the direction of power has to be maintained or should be changed.

B. SLIDING MODE ESC (SM-ESC) METHOD

This method is reported in [29]. This is an ESC method, which uses sliding mode control to generate the signals $u(\epsilon)$ and $v(\epsilon)$, where $u(\epsilon) = sign(\epsilon)$ and $v(\epsilon) = \epsilon + \delta$, where ϵ is the power error, and δ is a positive constant. A parameter M is selected taking into account the maximum derivative of the power with respect to the conductance of the PV module. The signal $v(\epsilon)$ and the parameter M are used to generate the PV power reference, while the signal $u(\epsilon)$ modifies the conductance g of the PV module.

C. STATIC CONDUCTANCE-BASED MPPT (SMPPT) METHOD

The SMPPT proposed in [30] has the objectives to track the global MPPT accurately and to eliminate the error between the reference and instantaneous PV module power $\epsilon(t) = P_{pref}(t) - P_{pv}(t)$. These objectives are achieved by modifying the conductance g of the PV module. The MPPT parameters are tuned taking into account the maximum derivative of the power with respect to the PV conductance.

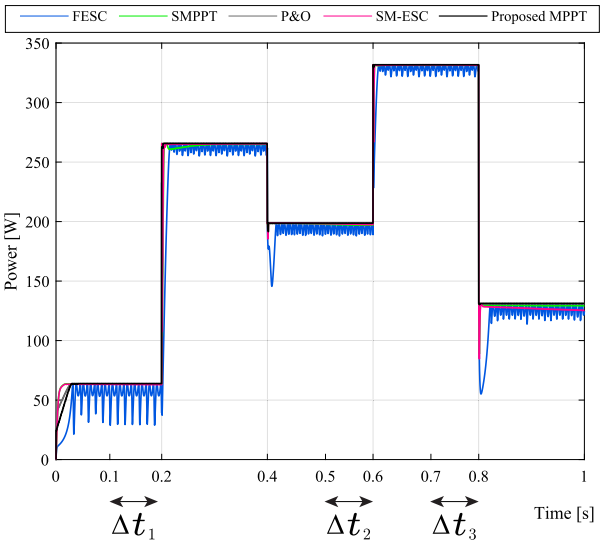

FIGURE 3. Simulated results comparing performances of MPPT methods.

D. CONVENTIONAL PERTURB AND OBSERVE (P&O) METHOD

This method has been widely used due to its simplicity and low cost [31]–[33]. The method compares the current measured power P[n] with its previous sampled value P[n − 1] and the voltage of the PV module with the maximum voltage to predict the MPP. A small step of reference voltage results in a power step of the PV module. If the power change is positive, the voltage change is continued in the same direction. If the power step is negative, it indicates that the current operating point is moving away from the MPP and the reference PV voltage has to be changed in the reverse direction to come closer to the MPP [31].

E. COMPARATIVE STUDY OF THE MPPT METHODS

All the methods were compared in PSIM using the solar module (physical model) that can take into account variations of the irradiance and ambient temperature. The characteristics of the case study PV corresponds to the PV module VBHN330SJ47 from Panasonic and are described in the next section. Overall simulated results of MPPT tracking accuracy are presented in Figure 8, where the irradiance changes from 200 W/m^2 to 800 W/m^2 at 0.2 s, from 800 W/m^2 to 600 W/m^2 at 0.4 s, from 600 W/m^2 to 1000 W/m^2 at 0.6 s, and from 1000 W/m^2 to 400 W/m^2 at 0.8 s. The temperature is 25°C. Figure 4 shows a zoom from Figure 8 for three values of the solar irradiance in the periods: Δt_1, Δt_2 and Δt_3. The MPPT efficiency values are summarized in Table. 1, which were calculated using the following equation:

$$\eta_{MPPT} = \frac{1}{T_m} \sum \frac{v_{pv} i_{pv}}{P_{mpp}} \Delta T \tag{38}$$

where P_{mpp} is the available MPP power of the solar module, ΔT is the sampling time (1 ms in these simulations), and

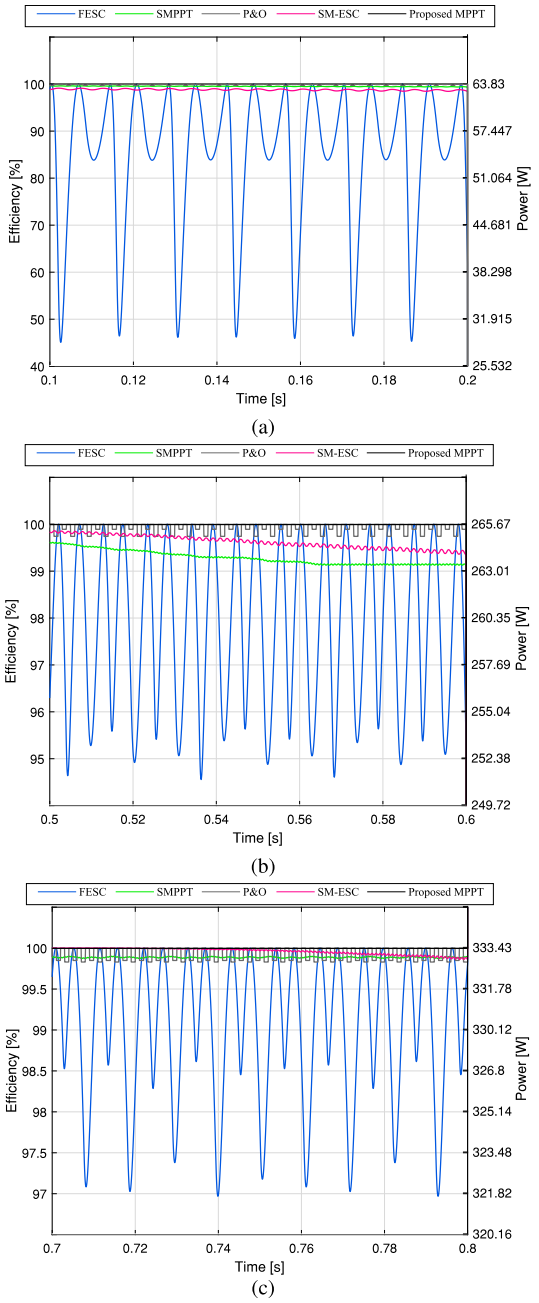

FIGURE 4. Steady-state simulated results of MPPT methods for three different irradiance levels IR: IR = 200 W/m^2 corresponds with Δt_1 (a), IR = 600 W/m^2 corresponds with Δt_2 (b), IR = 1000 W/m^2 corresponds with Δt_3 (c).

T_m is the overall measurement time interval. The proposed algorithm shows the best performance as its average tracking accuracy is the highest in all the intervals. It exceeds 99.84% and has the best transient response under irradiance step changes. The simulation results shown in this article are consistent with the comparative study presented in [30] for the ESC methods, where the MPPT efficiency results are over 90%, and the SMPPT showed the highest values of over 98.93%.

TABLE 1. MPPT efficiency.

MPPT	η_{total} [%]	$\eta_{\Delta t_1}$ [%]	$\eta_{\Delta t_2}$ [%]	$\eta_{\Delta t_3}$ [%]
FESC	92.14	84.99	97.83	99.02
SMPPT	98.93	99.47	99.26	99.85
P&O	99.38	99.85	99.88	99.88
SM-ESC	98.58	98.76	99.60	99.93
Proposed	99.84	99.96	99.98	99.96

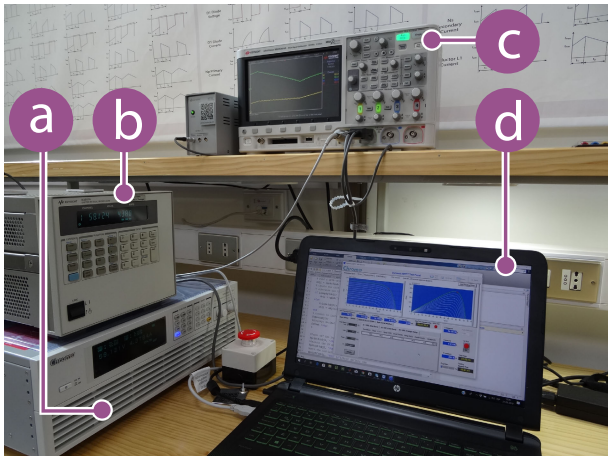

FIGURE 5. Experimental setup of the solar panel simulator: (a) Chroma 62050H-600S Programmable DC Power Supply with Solar Array Simulation controlled through a universal serial bus (USB) communication interface, (b) Keysight N3304A electronic load operating in constant voltage mode whose reference is provided by means of a general purpose interface bus (GPIB) communication interface, (c) Keysight MSOX2014A oscilloscope, (d) laptop with an MPPT algorithm implemented in MATLAB to control the electronic load and a Chroma solar array simulation soft panel.

V. HARDWARE-IN-THE-LOOP (HIL) TESTING

Once the correct operation of the proposed MPPT method has been validated using SIL, it has to be tested under real operating conditions. The Hardware-in-the-loop (HIL) testing system consists of:

- An electronic load Keysight N3304A configured in constant voltage mode.
- A programmable solar array simulator power supply Chroma 62050H-600S.
- A laptop with the MATLAB software.
- An oscilloscope Keysight MSOX2014A.

The electronic load was configured to operate in the constant voltage mode. The MPPT algorithm running in MATLAB (Algorithm 3) sets the reference voltage for the electronic load. The communication between the electronic load and the MATLAB run on a laptop is implemented using the general purpose interface bus (GPIB). Several minor procedures were used to interact with the electronic load. The Write-V procedure sends the voltage reference to the electronic load. The Read-IV procedure obtains the voltage and current at the operating point to evaluate the MPPT algorithm in the MATLAB. Reading the voltage is an additional safety measure that allows for detecting if the electronic load can

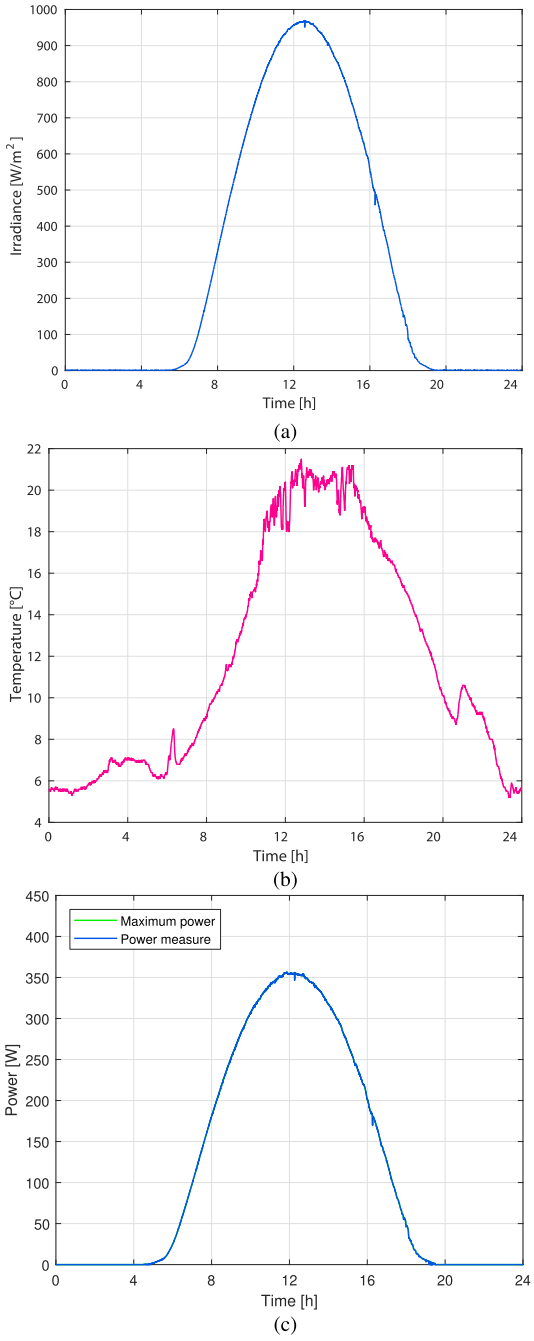

FIGURE 6. Clear day mission profile: (a) irradiance, (b) temperature, (c) power.

regulate its voltage according to the reference. In practice, the procedures will be modified since the electronic load will be substituted by a dc-dc switching converter such as [34], whose input voltage (the PV module voltage) is regulated in the closed loop, decoupling in this way the PV module from its load (for instance a battery). We are assuming that the response of the PV module voltage to a step-like reference change could exhibit settling times ranging from hundreds of milliseconds to some seconds. In this study, the settling time of 100 ms was found sufficiently long. It was added as

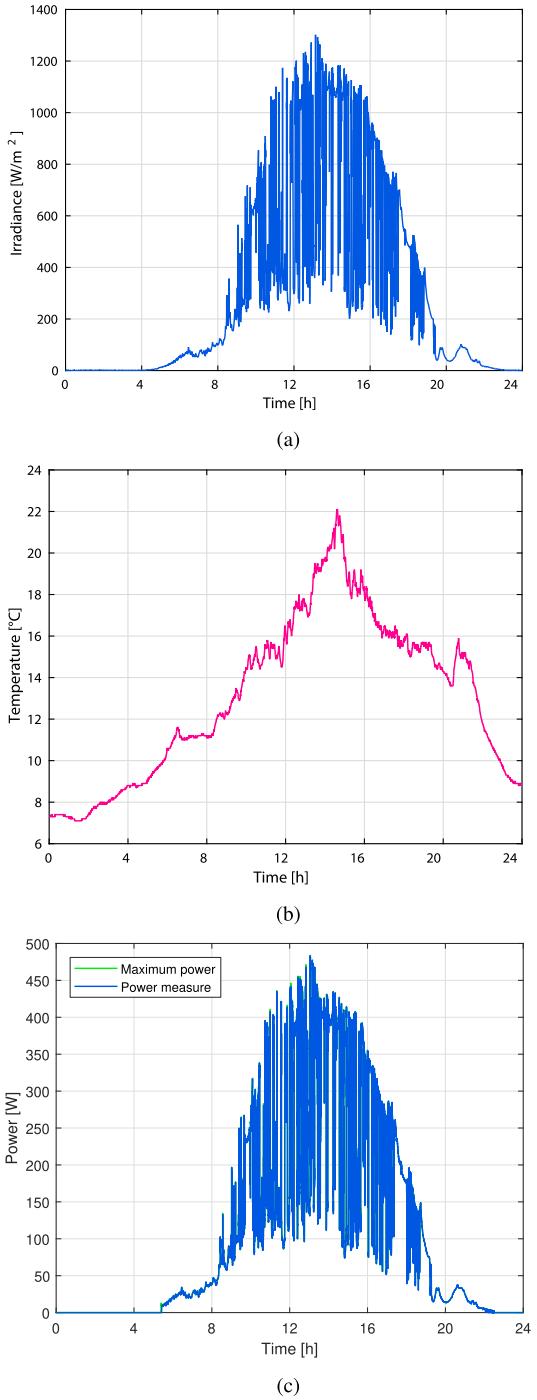

FIGURE 7. Cloudy day mission profile: (a) irradiance, (b) temperature, (c) power.

a software delay to the Write-V procedure. In the real implementation, the voltage will be measured and the program flow will be stopped until it reaches the reference value or a watchdog time is exceeded. With regards to the real measurements, all classical solutions to mitigate undesired switching noise effects can be used: low pass filter before the ADC stage, averaging several consecutive samples, synchronizing the sampling instants with the pulse width modulation signals, etc.

The used solar array simulator can emulate an arbitrary $i - v$ curve accurately and perform realistic tests by taking into account the influence of various weather conditions such as irradiance and temperature from the early morning to nightfall. This power supply can be controlled through a remote digital interface (USB, GPIB, Ethernet, RS232) using a graphical user interface software. The real-world weather simulation function allows to import real daily mission profiles of the solar irradiance and temperature to emulate the real operating conditions from early morning to nightfall. In addition, it can implement performance dynamic standard curves (EN50530, Sandia, CGC/GF004, CGC-GF035, NB/T 32004) as well as testing and monitoring the MPPT performance in real-time.

A laptop with the MPPT algorithm implemented in the MATLAB software was used to control the electronic load (GPIB communication) and the solar array simulation interface for the configuration and monitoring of the power supply (USB communication). A digital oscilloscope was used to verify the correct operation of the experimental setup.

The experiments were carried out considering the setup for the photovoltaic emulator described previously and shown in Figure 5. The PV characteristic programmed within the solar array simulator power supply corresponds to the PV module VBHN330SJ47 from Panasonic. The PV module parameters are: $P_{max} = 330$ W, $V_{mpp} = 58$ V, $I_{mpp} = 5.7$ A, $V_{oc} = 69.7$ V, $I_{sc} = 6.07$ A, temperature coefficient for open circuit voltage -0.17 V/°C, and temperature coefficient for short circuit current 0.002 A/°C.

Two daily mission profiles extracted from annual high resolution mission profiles of solar irradiance and temperature that were recorded in Aalborg, Denmark, and statistically analyzed in [35]. The cloudy day mission profile was recorded on July 2, while the clear day mission profile corresponds to March 21. The power output and MPP performance test for the clear day mission profile is shown in Figure 6. The proposed algorithm presented a tracking efficiency of 100% under the given irradiance (Figure 6 (a)) and temperature (Figure 6 (b)) changes. A similar test is presented in Figure 7 for the cloudy day mission profile. The tracking efficiency for the cloudy day equals 99.53%. The PV module generates 2508.1 Wh for the cloudy day mission profile and 2873.6 Wh for the clear day profile.

VI. PRELIMINARY MODIFICATIONS TO ADAPT THE ALGORITHM TO SHADING CONDITIONS

Figure 8 depicts the results obtained by a modification of the algorithms to deal with partial shading conditions. A Shading-conditions procedure is selected at the main procedure when the absolute difference between the measured current and the theoretical prediction at the MPP reaches a larger threshold than in normal operation. In the figure, when partial shading is detected, the Three-Points procedure is used to determine the MPPs in each of the four intervals of the

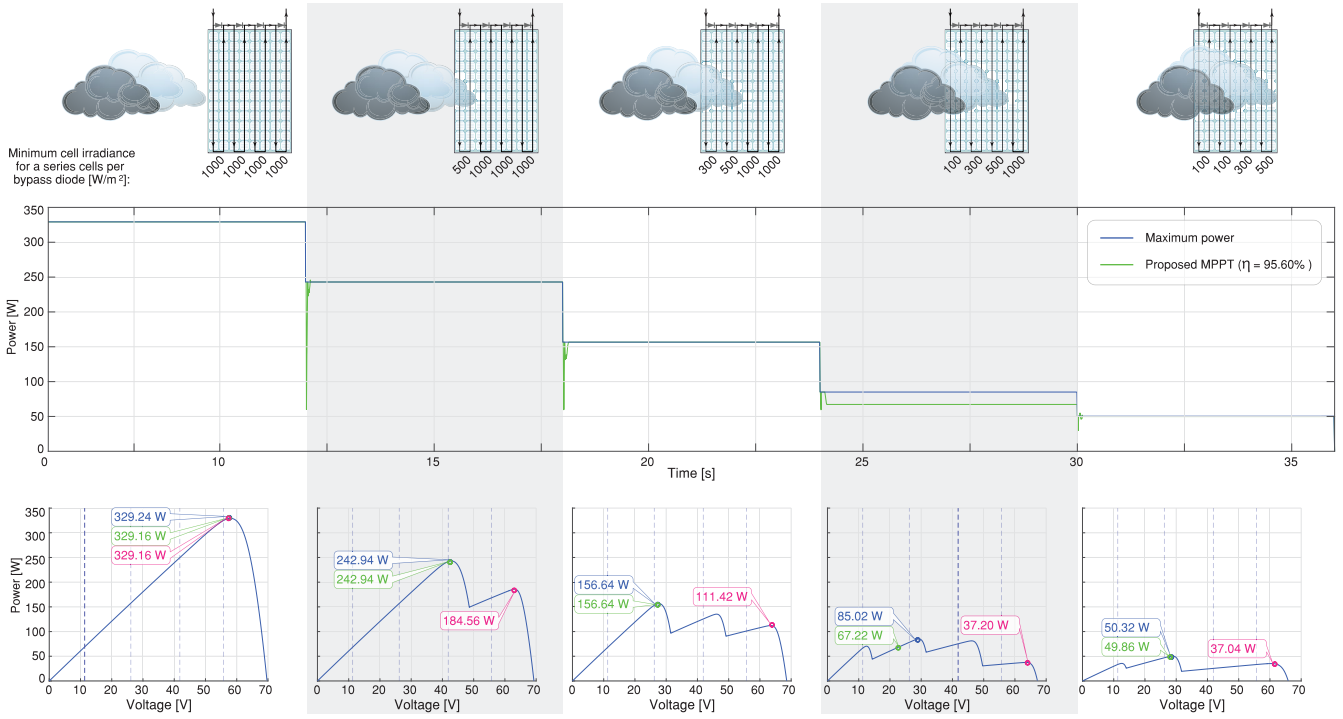

FIGURE 8. Preliminary results provided by a modified version of the algorithms to address partial shading operation causing activation of bypass diodes. Top subfigure: graphical representation of a progressive shading defining five different operating conditions. Middle subfigure: temporal evolution of the MPPs. Bottom: static $p - v$ curves of each interval. Traces and labels in blue correspond to the ideal MPP. Green color corresponds to the power obtained using the algorithm modified to address partial shading. The magenta labels color corresponds to the MPP obtained by the initial non-modified algorithm.

$p - v$ curve in which the selected PV module (with three bypass diodes) can have a local peak. Vertical lines show the initial voltage values at which the Three-Points algorithms are started. The figure illustrates the path of a cloud blocking the PV module in such a way that the bypass diodes are activated in a sequence (none-1-2-3-2) that results in the $p - v$ curves shown at the bottom. The figure also shows a $p - t$ evolution of the process where the theoretical maximum peaks are identified with blue dots. Green dots identify the MPPs identified by the proposed algorithm, while pink dots correspond with the maximums identified by the algorithm without any modification to adapt it to shading conditions. Please note that the assumed idealized abrupt activation of the bypass diodes occurs at 12 s intervals. The proposed algorithm has been able to detect correctly the absolute MPP in four of the five intervals shown. A post analysis has shown that the algorithm has not detected the correct MPP operation point in the fourth interval because the initial point was not adequate. Further efforts to eliminate this problems are currently ongoing. In a similar way, executing the P&O algorithm after the Three-Point Procedure to determine that the predicted MPP is really a peak and then refine the MPP position by the Two-Points algorithm is a possible solution.

VII. CONCLUSION

Simulations and hardware-in-the-loop experimental tests have shown that the proposed three-parameter model-based MPPT method compares successfully with other published high-performance methods in terms of MPPT efficiency. The basic method that requires measuring three voltage and current points in the vicinity of the MPP corresponding to the same $i-v$ curve, provides good MPP tracking results in static and slow varying MPPT dynamic tests. The algorithm has been optimized so that in many occasions only two parameters need to be identified, which requires measuring only one additional operation point, making it also suitable in fast irradiance and temperature dynamic conditions. A work in progress addresses the combination of the algorithm with a supervising procedure able to deal with multipeak $i-v$ curves caused by the activation of bypass diodes in partial shading operating conditions. Preliminary simulations of the modified method provide promising results in ideal shading conditions and the extension to more realistic environmental conditions is a work in progress.

ACKNOWLEDGMENT

The authors would like to acknowledge Dr. Oswaldo Lopez-Santos, Professor leader of the Research Group D + Tec (Technological Development), Universidad de Ibagué, Colombia for contributing with data to carry out some simulations.

REFERENCES

[1] J. Mayer, D. Fuerstenwerth, S. Philipps, N. S. Hussein, T. Schlegl, and C. Senkpiel, *Current and Future Cost of Photovoltaics*. Freiburg im Breisgau, Germany: Fraunhofer ISE, 2015

[2] M. A. Green, E. D. Dunlop, J. Hohl-Ebinger, M. Yoshita, N. Kopidakis, and A. W. Y. Ho-Baillie, "Solar cell efficiency tables (version 55)," *Prog. Photovolt., Res. Appl.*, vol. 28, no. 1, pp. 3–15, 2020.

[3] M. B. Hayat, D. Ali, K. C. Monyake, L. Alagha, and N. Ahmed, "Solar energy–A look into power generation, challenges, and a solar-powered future," *Int. J. Energy Res.*, vol. 43, no. 3, pp. 1049–1067, Mar. 2019.

[4] A. Pozza and T. Sample, "Crystalline silicon PV module degradation after 20 years of field exposure studied by electrical tests, electroluminescence, and LBIC," *Prog. Photovolt., Res. Appl.*, vol. 24, no. 3, pp. 368–378, Mar. 2016.

[5] Y. Tang, B. Raghuraman, J. Kuitche, G. TamizhMani, C. E. Backus, and C. Osterwald, "An evaluation of 27+ years old photovoltaic modules operated in a hot-desert climatic condition," in *Proc. IEEE 4th World Conf. Photovoltaic Energy Conf.*, May 2006, pp. 2145–2147.

[6] M. N. H. Khan, M. Forouzesh, Y. P. Siwakoti, L. Li, T. Kerekes, and F. Blaabjerg, "Transformerless inverter topologies for single-phase photovoltaic systems: A comparative review," *IEEE J. Emerg. Sel. Topics Power Electron.*, vol. 8, no. 1, pp. 805–835, Mar. 2020.

[7] W. Li and X. He, "Review of nonisolated high-step-up DC/DC converters in photovoltaic grid-connected applications," *IEEE Trans. Ind. Electron.*, vol. 58, no. 4, pp. 1239–1250, Apr. 2011.

[8] D. G and S. N. Singh, "Selection of non-isolated DC-DC converters for solar photovoltaic system," *Renew. Sustain. Energy Rev.*, vol. 76, pp. 1230–1247, Sep. 2017.

[9] W. Van De Sande, S. Ravyts, O. Alavi, P. Nivelle, J. Driesen, and M. Daenen, "The sensitivity of an electro-thermal photovoltaic DC–DC converter model to the temperature dependence of the electrical variables for reliability analyses," *Energies*, vol. 13, no. 11, p. 2865, Jun. 2020.

[10] Y. Shen, A. Chub, H. Wang, D. Vinnikov, E. Liivik, and F. Blaabjerg, "Wear-out failure analysis of an impedance-source PV microinverter based on system-level electrothermal modeling," *IEEE Trans. Ind. Electron.*, vol. 66, no. 5, pp. 3914–3927, May 2019.

[11] *European Committee for Electrotechnical Standardization. Overall efficiency of grid connected Photovoltaic Inverters*, Standard EN 50530:2010 A1:2013, European Committee for Standardization, Brussels, Belgium, 2013.

[12] A. Chub, O. Korkh, R. Kosenko, and D. Vinnikov, "Novel approach immune to partial shading for photovoltaic energy harvesting from building integrated PV (BIPV) solar roofs," in *Proc. 20th Eur. Conf. Power Electron. Appl. (EPE ECCE Europe)*, Sep. 2018, pp. P.1–P.10.

[13] A. Ali, K. Almutairi, S. Padmanaban, V. Tirth, S. Algarni, K. Irshad, S. Islam, M. H. Zahir, M. Shafiullah, and M. Z. Malik, "Investigation of MPPT techniques under uniform and non-uniform solar irradiation condition—A retrospection," *IEEE Access*, vol. 8, pp. 127368–127392, 2020.

[14] A. Anurag, S. Bal, S. Sourav, and M. Nanda, "A review of maximum power-point tracking techniques for photovoltaic systems," *Int. J. Sustain. Energy*, vol. 35, no. 5, pp. 478–501, 2016.

[15] T. Esram and P. L. Chapman, "Comparison of photovoltaic array maximum power point tracking techniques," *IEEE Trans. Energy Convers.*, vol. 22, no. 2, pp. 439–449, Jun. 2007.

[16] M. A. Eltawil and Z. Zhao, "MPPT techniques for photovoltaic applications," *Renew. Sustain. Energy Rev.*, vol. 25, pp. 793–813, Sep. 2013.

[17] M. Abdel-Salam, M.-T. El-Mohandes, and M. Goda, "An improved perturb-and-observe based MPPT method for PV systems under varying irradiation levels," *Sol. Energy*, vol. 171, pp. 547–561, Sep. 2018.

[18] A. Reza Reisi, M. Hassan Moradi, and S. Jamasb, "Classification and comparison of maximum power point tracking techniques for photovoltaic system: A review," *Renew. Sustain. Energy Rev.*, vol. 19, pp. 433–443, Mar. 2013.

[19] S. Jain and V. Agarwal, "A new algorithm for rapid tracking of approximate maximum power point in photovoltaic systems," *IEEE Power Electron Lett.*, vol. 2, no. 1, pp. 16–19, Mar. 2004.

[20] M. A. G. de Brito, L. Galotto, L. P. Sampaio, G. D. A. Melo, and C. A. Canesin, "Evaluation of the main MPPT techniques for photovoltaic applications," *IEEE Trans. Ind. Electron.*, vol. 60, no. 3, pp. 1156–1167, Mar. 2013.

[21] A. K. Panchal, "A per-unit-single-diode-model parameter extraction algorithm: A high-quality solution without reduced-dimensions search," *Sol. Energy*, vol. 207, pp. 1070–1077, Sep. 2020.

[22] G. Petrone, M. Luna, G. La Tona, M. Di Piazza, and G. Spagnuolo, "Online identification of photovoltaic source parameters by using a genetic algorithm," *Appl. Sci.*, vol. 8, no. 1, p. 9, Dec. 2017.

[23] D. Veberič, "Lambert w function for applications in physics," *Comput. Phys. Commun.*, vol. 183, no. 12, pp. 2622–2628, Dec. 2012.

[24] W. Xiao, M. G. J. Lind, W. G. Dunford, and A. Capel, "Real-time identification of optimal operating points in photovoltaic power systems," *IEEE Trans. Ind. Electron.*, vol. 53, no. 4, pp. 1017–1026, Jun. 2006.

[25] A. Capel, "Circuit and method for controlling the point of maximum power for solar energy source and solar generator incorporating said circuit," U.S. Patent 20 100 176 773 A1, Mar. 30, 2007.

[26] A. Capel, "Process to operate continuously a solar array to its maximum power in variable shadowing conditions and device needed to carry it out," Worldwide Patent 2 012 010 203 A1, Jul. 2010.

[27] A. Capel, "Management of a photovoltaic power system by a power conditioning unit (PCU) calculating the maximum power point (MPPC)," France Patent 3 050 548 B1, Apr. 2016.

[28] R. Haroun, A. El Aroudi, A. Cid-Pastor, G. Garcia, C. Olalla, and L. Martinez-Salamero, "Impedance matching in photovoltaic systems using cascaded boost converters and sliding-mode control," *IEEE Trans. Power Electron.*, vol. 30, no. 6, pp. 3185–3199, Jun. 2015.

[29] A. H. Alqahtani and V. I. Utkin, "Self-optimization of photovoltaic system power generation based on sliding mode control," in *Proc. IECON 38th Annu. Conf. IEEE Ind. Electron. Soc.*, Oct. 2012, pp. 3468–3474.

[30] O. Lopez-Santos, G. Garcia, L. Martinez-Salamero, R. Giral, E. Vidal-Idiarte, M. C. Merchan-Riveros, and Y. Moreno-Guzman, "Analysis, design, and implementation of a static conductance-based MPPT method," *IEEE Trans. Power Electron.*, vol. 34, no. 2, pp. 1960–1979, Feb. 2019.

[31] M. Kamran, M. Mudassar, M. R. Fazal, M. U. Asghar, M. Bilal, and R. Asghar, "Implementation of improved perturb & observe MPPT technique with confined search space for standalone photovoltaic system," *J. King Saud Univ. Eng. Sci.*, vol. 32, no. 7, pp. 432–441, Nov. 2020.

[32] E. M. Varaprasad and N. Sriharish, "A novel adaptive P&O MPPT algorithm considering sudden changes in the irradiance," *IEEE Trans. Energy Convers.*, vol. 29, no. 3, pp. 602–610, Sep. 2014.

[33] J. Ahmed and Z. Salam, "A modified P&O maximum power point tracking method with reduced steady-state oscillation and improved tracking efficiency," *IEEE Trans. Sustain. Energy*, vol. 7, no. 4, pp. 1506–1515, Oct. 2016.

[34] F. Mendez-Diaz, B. Pico, E. Vidal-Idiarte, J. Calvente, and R. Giral, "HM/PWM seamless control of a bidirectional buck–boost converter for a photovoltaic application," *IEEE Trans. Power Electron.*, vol. 34, no. 3, pp. 2887–2899, Mar. 2019.

[35] Chub, Vinnikov, Stepenko, Liivik, and Blaabjerg, "Photovoltaic energy yield improvement in two-stage solar microinverters," *Energies*, vol. 12, no. 19, p. 3774, Oct. 2019.

CARLOS RESTREPO received the bachelor's degree (Hons.) and the master's degree in electrical engineering from the Universidad Tecnológica de Pereira, Colombia, in 2006 and 2007, respectively, and the master's and Ph.D. (Hons.) degrees in electronic engineering from the Universitat Rovira i Virgili de Tarragona, Tarragona, Spain, in 2008 and 2012, respectively.

He was a Visiting Scholar with the Faculty of Electrical Engineering and Computer Science, University of Maribor, Slovenia, in 2011. From 2013 to 2014, he was a Post-Doctoral Researcher with the Electrical Power Processing Group, Delft University of Technology, Delft, The Netherlands. From 2014 to 2016, he was a Professor with the Departamento de Ingeniería Eléctrica, Universidad Técnica Federico Santa María, Santiago, Chile. He is currently a Professor with the Departamento de Ingeniería Eléctrica, Universidad de Talca, Curicó, Chile. His main research interests include modeling and emulator design for fuel cells, design and digital control of switched converters, and energy management of hybrid electric vehicles. He is currently the Director of the Laboratory of Applications in Smart Grids Research Group.

CATALINA GONZÁLEZ-CASTAÑO received the degree in electronic engineering from the Universidad Nacional de Colombia, Manizales, and the M.Eng. degree in electrical engineering from the Universidad Tecnológica de Pereira, Colombia, in 2008 and 2013, respectively, and the Ph.D. degree (Hons.) in electronic engineering with a focus on power converters for electric vehicles from the Universitat Rovira i Virgili, Tarragona, Spain, in 2019. She was a Ph.D. Intern with the Advanced Center of Electrical and Electronic Engineering, Valparaiso, Chile. Her main research interests are electric power quality, vehicular power systems, and design and digital control of power converters.

JAVIER MUÑOZ (Member, IEEE) received the B.S. degree (Hons.) in electronic engineering and the M.S. and Ph.D. degrees in electrical engineering from the University of Concepcion, Concepcion, Chile, in 2007, 2009, and 2012, respectively. Since 2011, he has been with the University of Talca, Curicó, Chile, where he is currently the Dean of the Faculty of Engineering. His current research and teaching interests include dynamic systems and microinverters for photovoltaic integration to the grid.

ANDRII CHUB (Senior Member, IEEE) received the B.Sc. and M.Sc. degrees from Chernihiv State Technological University, Chernihiv, Ukraine, in 2008 and 2009, respectively, and the Ph.D. degree in electrical engineering from the Tallinn University of Technology (TalTech), Estonia, in 2016. He is currently a Senior Researcher with the Power Electronics Group, TalTech. He was a Visiting Research Fellow with Kiel University in 2017 and a Post-Doctoral Researcher with Federico Santa Maria Technical University from 2018 to 2019. He has coauthored over 100 articles and book chapters on power electronics and applications. He also holds several patents and utility models. His research interests include dc–dc converters, dc microgrids, renewable energy conversion systems for energy-efficient residential buildings, fault tolerance, and reliability in power electronic systems. He received numerous best paper awards at the IEEE conferences and the 2018 Industrial Electronics Society Best Conference Paper Award. He is an Associate Editor of the IEEE JOURNAL OF EMERGING AND SELECTED TOPICS IN INDUSTRIAL ELECTRONICS.

ENRIC VIDAL-IDIARTE (Member, IEEE) received the Licenciado en Informática and Ph.D. degrees from the Universitat Politècnica de Catalunya, Barcelona, Spain, in 1993 and 2001, respectively. He is currently an Associate Professor with the Departament d'Enginyeria Electrònica, Elèctrica i Automàtica, Escola Tècnica Superior d'Enginyeria, Universitat Rovira i Virgili, Tarragona, Spain, where he is working in the field of digital and robust control of power converters. He is a also member of the Grup d'Automàtica i Electrònica Industrial Research Group on Industrial Electronics and Automatic Control, whose main research fields are power conditioning for vehicles, satellites, and renewable energy.

ROBERTO GIRAL (Senior Member, IEEE) received the B.S. degree in ingeniería técnica de telecomunicación and the M.S. and Ph.D. (Hons.) degrees in ingeniería de telecomunicación from the Universitat Politècnica de Catalunya, Barcelona, Spain, in 1991, 1994, and 1999, respectively. He is currently an Associate Professor with the Departament d'Enginyeria Electrònica, Elèctrica i Automàtica, Escola Tècnica Superior d'Enginyeria, Universitat Rovira i Virgili, Tarragona, Spain, where he is working in the field of power electronics. He is also the Director of the Grup d'Automàtica i Electrònica Industrial Research Group.